Vibrational Analysis of Peptides, Polypeptides, and Proteins. XVIII. Conformational Sensitivity of the α-Helix Spectrum: α_I- and α_{II}-Poly(L-alanine)

ANIL M. DWIVEDI and S. KRIMM, *Biophysics Research Division, University of Michigan, Ann Arbor, Michigan 48109*

Synopsis

The α_{II}-helix ($\phi = -70.47°$, $\psi = -35.75°$) is a structure having the same n and h as the (standard) α_I-helix ($\phi = -57.37°$, $\psi = -47.49°$). Its conformational angles are commonly found in proteins. Using an improved α-helix force field, we have compared the vibrational frequencies of these two structures. Despite the small conformational differences, there are significant predicted differences in frequencies, particularly in the amide A, amide I, and amide II bands, and in the conformation-sensitive region below 900 cm^{-1}. This analysis indicates that α_{II}-helices are likely to be present in bacteriorhodopsin [Krimm, S. & Dwivedi, A. M. (1982) *Science* **216**, 407–408].

INTRODUCTION

Our recent work on β-sheet polypeptides[1,2] and on β-turns[3–8] has amply demonstrated the sensitivity of the vibrational frequencies of such molecules to relatively large changes in the conformation. Our earlier work on α-helical poly(L-alanine)[9] [α-$(Ala)_n$] had also shown that the α-helix frequencies can be sensitive to small changes in conformation. In this case, it is the result of changing h, the rise per residue, by a very small amount while keeping n, the number of residues per turn, constant. Such small structural changes seemed to be responsible for frequency changes that occur as a result of changing the temperature of the sample.[9]

In the present study, we were interested in a specific and relatively small conformational change that the α-helix can undergo at constant n and h. This occurs because, in general, there are two possible solutions for the dihedral angles ϕ and ψ when the above helix parameters are kept constant.[10] One of these solutions corresponds to the standard helix, which we designate the α_I-helix, and the other is a slightly modified structure, which we designate the α_{II}-helix. These differ primarily in that in the α_{II}-helix, the plane of the peptide group has more tilt with respect to the helix axis, resulting in an N—H bond that distinctly points toward the axis. The consequence is a bent N—H···O=C hydrogen bond, and in extreme cases, an N···O distance that is inconsistent with a hydrogen bond.[11]

Although the difference in ϕ,ψ is small, x-ray crystallographic data on several proteins indicate that there are α-helical segments that have dihedral angles corresponding to the α_{II} conformation: three segments (residues 29–35, 93–99, and 120–124) in lysozyme,[12] two segments (residues

Biopolymers, Vol. 23, 923–943 (1984)
© 1984 John Wiley & Sons, Inc. CCC 0006-3525/84/050923-21$04.00

165–172 and 237–243) in α-chymotrypsin,[13] and one segment (residues 28–31) in chromatium high-potential iron protein.[14] In fact, the conformation of α-$(Ala)_n$ in hexafluoroisopropanol has been shown to be incompatible with an α_I-helix, and an α_{II}-helix conformation has been proposed[15] in this solvent. It is therefore important to understand the spectroscopic characteristics of these two structures and, in particular, to know whether the vibrational spectrum is sensitive to such small conformational changes.

The force field used in this calculation differs from that developed previously for α-$(Ala)_n$.[9] The main reasons for doing this further refinement of the force field were to incorporate a better-defined x-ray structure,[16] to include a complete set of hydrogen-bond force constants, and, in the spirit of our earlier work on β-sheet polypeptides,[1,2] to employ a force field with maximum transferability between different conformations. We have therefore done a refinement for α_I-$(Ala)_n$ based on the transfer of force constants from β-$(Ala)_n$ [2] and a consistent prediction of the frequencies of α_I-$(Ala\text{-}ND)_n$. This force field was then used to calculate the frequencies of α_{II}-$(Ala)_n$. During this study, we observed that certain anomalies in the ir spectrum of the purple membrane of *Halobacterium halobium*[17,18] could be accounted for by the α_{II} conformation, and a preliminary description of these conclusions, and their possible relevance to the proton conduction mechanism of this protein, has been reported.[19]

NORMAL-MODE CALCULATION

Structure

The helix parameters for the α_I-helix are the same as those used in our earlier work,[9] viz., $n = 3.62$, $h = 1.495$ Å, and t (rotation per residue about the helical axis) = 99.57°, as are the bond lengths and bond angles.[2,9] However, there is a significant difference in the dihedral angles. In this work, we have used values $\phi = -57.37°$ and $\psi = -47.49°$ derived by Arnott and Dover[16] from an x-ray diffraction refinement procedure. In order to keep the helical parameters the same and use Arnott's ϕ,ψ, the value of τ (the $NC^{\alpha}C$ angle) has to be increased from the ideal tetrahedral value of 109.47° to 109.87°. Another important difference is in χ_1 (the rotation angle about the C^{α}—C^{β} bond). The value used earlier,[9] viz., $\chi_1 = 0°$, corresponds to an eclipsed position of a CH_3 group hydrogen atom with respect to the backbone N atom. We feel that a staggered position is more appropriate and have used $\chi_1 = 60°$, a value closer to that ($\chi_1 = 57.50°$) determined for β-$(Ala)_n$ by energy minimization.[20] A portion of the α_I-helix is shown in Fig. 1(a). The α_{II}-helix structure has been obtained using the second set of ϕ,ψ values[10] (−70.47°, −35.75°) that correspond to the same helical parameters as for α_I. The α_{II}- helix is shown in Fig. 1(b). As mentioned earlier, the peptide plane in α_{II} is tilted such that the C═O bond points away from the helix axis and the N—H bond points toward the helix

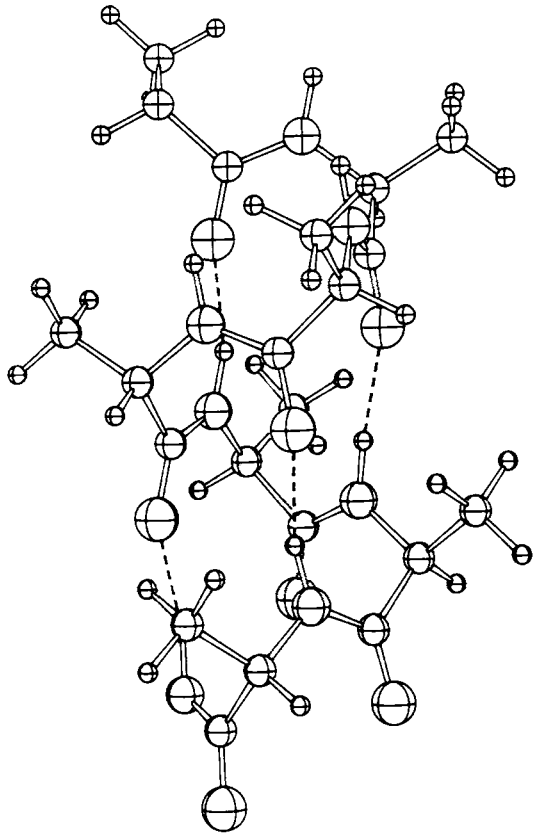

(a)

Fig. 1. α-Helical structures of poly(L-alanine): (a) α_I-helix, (b) α_{II}-helix.

axis. The results of such a structural change are that the hydrogen bonds are weaker in α_{II} than in α_I (for α_I: $r(H\cdots O) = 1.882$ Å, $r(N\cdots O) = 2.857$ Å, $\angle NHO = 164.19°$, $\angle HNO = 10.34°$; for α_{II}: $r(H\cdots O) = 2.121$ Å, $r(N\cdots O) = 3.001$ Å, $\angle NHO = 145.65°$, $\angle HNO = 23.51°$) and the distance between the H's of adjacent NH groups decreases, from 2.79 Å in α_I to 2.53 Å in α_{II}.

It may be worth noting that if the helical parameters are to remain the same, certain values of ϕ,ψ for the α_I-helix permit a much easier conversion to α_{II} than do others. If such flexibility is important (for example, allowing for a maximization of entropy), then these values for α_I will be favored (at present, variations of $\pm 8°$ in ϕ and ψ are commonly found in the literature). For example, whereas the α_I conformation that we use[16] leads to an α_{II} conformation that is comparably allowed,[21] the α_{II} conformation reported by Némethy et al.[11] ($-93°,-18°$), and based on standard bond lengths and angles as well as dihedral angles ($-53°,-52°$ for α_I), is not allowed.[21]

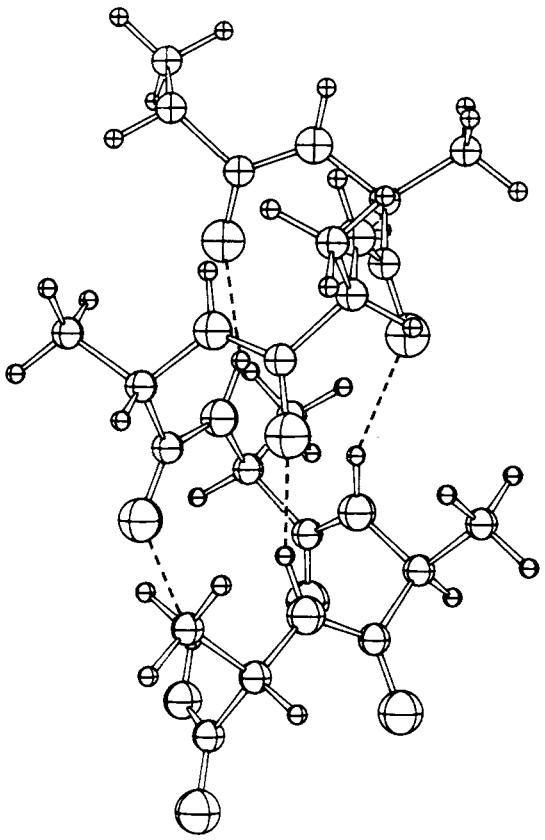

(b)

Fig. 1. (*continued from the previous page*)

For the normal-mode calculation, the internal and local symmetry coordinates of one chemical repeat unit have been defined in a way similar to that in the earlier work,[22] except that the $H^{\alpha}\cdots H^{\alpha}$ interchain stretching coordinate is not required for the α-helix. Thus, the chemical repeat unit has 39 internal coordinates compared with the 40 present in β-$(Ala)_n$.[2] It is worth pointing out that in the earlier work on α-$(Ala)_n$,[9] only 35 internal coordinates of the chemical repeat unit were used, the four intrachain internal coordinates NH···O and CO···H in-plane angle bends and NH···O and CO···H torsions having been neglected. Once the intrachain hydrogen bond is included in the calculation, a more complete treatment requires that the above-mentioned internal coordinates be included.

The optically active modes are classified into A ($\delta = 0°$), E_1 ($\delta = 99.57°$), and E_2 ($\delta = 199.14°$) symmetry species, where δ is the phase difference between the motions in adjacent residues. The former two species are both ir and Raman active and the last is Raman active only. In the ir dichroic spectrum, the A modes are parallel and the E_1 modes are perpendicular to the helical axis. There are 28A, $29E_1$, and $30E_2$ modes.[23]

Force Field

Except for the force constants associated with transition dipole coupling[24,25] and the $H^{\alpha}\cdots H^{\alpha}$ interaction, the force field for β-$(Ala)_n$ was used as a starting point[2] for the refinement of the α-$(Ala)_n$ force field. Appropriate changes were then made in some of the force constants in order to obtain more reasonable agreement between the predicted frequencies and the observed assigned bands. Most of the experimental data have been taken from our earlier work.[9] For the polarized ir and far-ir spectra, and the relative intensities, the results of other authors have also been used.[26-34] Transition dipole coupling constants were calculated using the same parameters as in the earlier work.[9] In the α_I-helix, the contributions to the A, E_1, and E_2 species for amide I are -5.53, -7.24, and -16.82 cm^{-1}, respectively, and for amide II they are -9.64, 6.17, and 4.23 cm^{-1}, respectively. In the α_{II}-helix, such contributions are -0.93, -8.06, and -13.38 cm^{-1} and -12.79, 7.43, and 5.97 cm^{-1}, respectively. The variations result from the conformational differences between these two structures.

As in the transfer of force constants from (Gly I)$_n$ (β-structure) to (Gly II)$_n$ (3_1-helix),[35] the required changes in force constants in transferring the force field from β-$(Ala)_n$ to α_I-$(Ala)_n$ can be attributed to the differences in conformation and in hydrogen-bond parameters between the two structures. Of a total of 98 force constants transferred from β-$(Ala)_n$, 35 required modification. A list comparing the unequal force constants of α- and β-$(Ala)_n$ is given in Table I. Eleven force constants—namely, f(CO), f(NH), $f(H\cdots O)$, $f(C^{\alpha}NH)$, f(CNH), $f(C^{\alpha}CO)$, $f(NH\cdots O$ ib), f(CO ob), f(NH ob), f(NCO), and f(CO ob,NH ob)—are directly influenced by the hydrogen bonds, and the differences in their values between α- and β-$(Ala)_n$ are due to the weaker hydrogen bonds in the former [$r(N\cdots O) = 2.857$ Å for α-$(Ala)_n$] as compared with the latter [$r(N\cdots O) = 2.732$ Å for β-$(Ala)_n$]. Fermi resonance analysis has been done for the amide A and amide B modes,[36] and f(NH) was adjusted so that the calculation predicts the unperturbed amide A frequency,[36] $\nu_A^{\circ} = 3279$ cm^{-1}. This value is significantly higher than that for β-$(Ala)_n$, viz., 3242 cm^{-1}, consistent with the expectation that a weaker hydrogen bond leads to a stronger N—H bond. The f(NH) and $f(H\cdots O)$ force constants for α-$(Ala)_n$ are 5.83 and 0.120 mdyn/Å, respectively, compared to 5.674 and 0.150 mdyn/Å for β-$(Ala)_n$. Except for $f(C^{\alpha}H^{\alpha})$, $f(H^{\alpha}C^{\alpha}C^{\beta})$, $f(C^{\alpha}C^{\beta}H)$, $f(C^{\alpha}C^{\beta}H,C^{\alpha}C^{\beta}H)$, and $f(C^{\alpha}C^{\beta}H,H^{\alpha}C^{\alpha}C^{\beta})_G$, the remaining 19 force constants in Table I reflect the conformational differences between β- and α-$(Ala)_n$. It is interesting that this number is about twice as large as the 10 conformation-dependent force constants that needed changing in going from (Gly I)$_n$ to (Gly II)$_n$.[35] The increase is not surprising, since in the latter case, only ϕ changes significantly [for (Gly I)$_n$ $\phi = 149.9°$ and $\psi = 146.5°$, compared with $\phi = -76.9°$ and $\psi = 145.3°$ for (Gly II)$_n$],[35] whereas the change from β-$(Ala)_n$ to α-$(Ala)_n$ involves a change in both ϕ and ψ, from $-138.38°$, 135.73° to $-57.37°$, $-47.49°$, respectively.[2] The force constant $f(C^{\alpha}H^{\alpha})$ had to be increased in α-$(Ala)_n$ in order to compensate for the absence of the $H^{\alpha}\cdots H^{\alpha}$

TABLE I
Comparison of Unequal Force Constants for α- and β-Poly(L-alanine)

Force Constant[a]	α[b]	β[b]
$f(NC^{\alpha})$	4.323	4.523
$f(CO)$	10.029	9.882
$f(NH)$	5.830	5.674
$f(C^{\alpha}H^{\alpha})$	4.523	4.463
$f(H\cdots O)$	0.120	0.150
$f((NC^{\alpha}C)$	1.119	0.819
$f(C^{\alpha}CN)$	1.033	0.933
$f(CNC^{\alpha})$	0.826	0.526
$f(NCO)$	1.446	1.306
$f(C^{\alpha}NH)$	0.556	0.566
$f(CNH)$	0.556	0.566
$f(C^{\alpha}CO)$	1.046	1.306
$f(CC^{\alpha}H^{\alpha})$	0.654	0.684
$f(H^{\alpha}C^{\alpha}C^{\beta})$	0.615	0.518
$f(C^{\alpha}C^{\beta}H)$	0.687	0.677
$f(NH\cdots O$ ib)	0.020	0.036
$f(CO$ ob)	0.657	0.621
$f(NH$ ob)	0.129	0.157
$f(NC^{\alpha}$ t)	0.087	0.037
$f(C^{\alpha}C$ t)	0.060	0.037
$f(NC^{\alpha},C^{\alpha}C)$	0.100	0.300
$f(NC^{\alpha},NC^{\alpha}H^{\alpha})$	0.427	0.627
$f(C^{\alpha}C,CC^{\alpha}H^{\alpha})$	0.305	0.205
$f(C^{\alpha}C,C^{\alpha}CO)$	0.100	0.200
$f(CO,C^{\alpha}CN)$	0.000	0.050
$f(C^{\alpha}C^{\beta},NC^{\alpha}C^{\beta})$	0.517	0.617
$f(NC^{\alpha}C,C^{\alpha}CN)$	0.160	0.000
$f(NC^{\alpha}C,CO$ ob)	−0.073	−0.173
$f(NC^{\alpha}C,NH$ ob)	0.160	0.110
$f(NC^{\alpha}C^{\beta},C^{\alpha}C^{\beta}H)_G$	0.000	0.040
$f(CC^{\alpha}H^{\alpha},CO$ ob)	−0.100	0.150
$f(CC^{\alpha}C^{\beta},CO$ ob)	−0.050	0.162
$f(C^{\alpha}C^{\beta}H,C^{\alpha}C^{\beta}H)$	−0.020	−0.045
$f(C^{\alpha}C^{\beta}H,H^{\alpha}C^{\alpha}C^{\beta})_G$	0.000	0.100
$f(CO$ ob,NH ob)	−0.050	0.000

[a] f(AB) = AB bond stretch, f(ABC) = ABC angle bend, f(X,Y) = XY interaction; ib = in-plane bend, ob = out-of-plane bend, t = torsion, G = *gauche*.

[b] Units are mdyn/Å for stretch and stretch, stretch force constants, mdyn for stretch, bend force constants, and mdyn Å for all others.

interaction. Although we do not have a good understanding of the reasons for changes in $f(H^{\alpha}C^{\alpha}C^{\beta})$, $f(C^{\alpha}C^{\beta}H)$, $f(C^{\alpha}C^{\beta}H,C^{\alpha}C^{\beta}H)$, and $f(C^{\alpha}C^{\beta}H,H^{\alpha}C^{\alpha}C^{\beta})_G$, we were forced to modify these force constants. This was a consequence of the low predicted frequency for a band observed near 1310 cm^{-1} and assignable to H^{α} bend, as is a similar band in β-$(Ala)_n$. In order to raise the low predicted value in α-$(Ala)_n$, and to keep an assignment similar to that in β-$(Ala)_n$, the $f(C^{\alpha}C^{\beta}H,H^{\alpha}C^{\alpha}C^{\beta})_G$ force constant, which

was found to be the most influential, had to be reduced to zero. When this was done, the other three force constants required only slight adjustments.

It should be noted that this refinement preserves a high degree of transferability in the basic force field. When we consider α_I-(Ala)$_n$ in the context of the global refinement for (Gly I)$_n$,[1] (Gly II)$_n$,[35] β-(Ala)$_n$,[2] and β-(Ala Gly)$_n$ (unpublished results), we find that about 550 frequencies have been fitted by 193 values in a set of 113 force constants. The observed frequencies below 1700 cm^{-1} are predicted with an average error of about 5 cm^{-1}, which suggests that conformational changes giving rise to larger frequency differences than this should be determinable from the vibrational spectrum.

For the α_{II}-helix, all of the above force constants were used without alteration, except for f(CO), f(NH), and f(H$\cdots$O). The hydrogen-bond force constant was given a value, f(H$\cdots$O) = 0.0858, that is proportional to the r(N$\cdots$O) distance in the α_{II}-helix, using the comparable values in β-(Ala)$_n$ (Ref. 2) and the α_I-helix for purposes of extrapolation. The other two force constants have to be increased, since the hydrogen bond is weaker in α_{II} than in α_I; the particular values chosen, viz., f(CO) = 10.129 and f(NH) = 5.908, brought the respective frequencies into agreement with the observations on the ir spectra of *H. halobium*.[17,18] Splittings in the amide I and amide II modes due to transition dipole coupling were calculated using the same parameters as for the α_I-helix but with the geometry of the α_{II}-helix.

RESULTS AND DISCUSSION

α_I-Poly(L-alanine)

It is appropriate to note first how well the new force field predicts the spectrum of α_I-(Ala)$_n$ before considering its application to studying the α_I to α_{II} conformational change. The calculated and observed frequencies of (Ala)$_n$ and (Ala-ND)$_n$ in the α_I conformation are listed in Table II.

As mentioned earlier, Fermi resonance analysis[36] gives an unperturbed amide A mode, ν_A° = 3279 cm^{-1}, which was used to refine the value of f(NH). When the same force constant is used to calculate ν(ND), it gives a value of 2409 cm^{-1}, about 40 cm^{-1} lower than the observed ν_A°(ND),[36] viz., 2449 cm^{-1}. This is similar to the case of β-(Ala-ND)$_n$,[2] for which the calculated value of the ND stretch is about 50 cm^{-1} lower than the observed ν_A°(ND), and is explainable by the presence of different anharmonicities in (Ala)$_n$ and (Ala-ND)$_n$. In the CH stretching region, the agreement with the observed values is quite good for the CH_3 antisymmetric and $C^\alpha H^\alpha$ modes, but the calculation does not reproduce the splittings of ~12 cm^{-1} in the CH_3 symmetric stretch region. As suggested earlier,[9] this discrepancy may be due to the presence of $CH_3\cdots CH_3$ nonbonded interactions between the

TABLE II
Observed and Calculated Frequencies (in cm^{-1}) of α_I-Poly(L-alanine)

Observed[a]		Calculated			
Raman	ir	A	E_1	E_2	Potential Energy Distribution[b]
			$[NHCH(CH_3)CO]_n$		
	3279VS ∥[c]	3279	3279	3279	NH s(98)
		2984			CH_3 as1(96)
			2984		CH_3 as1(99)
				2984	CH_3 as1(98)
2988S	2983VS ∥	2984			CH_3 as2(96)
			2984		CH_3 as2(99)
				2984	CH_3 as2(98)
2930M,sh	2925M ∥	2930			CH_3 ss(100)
2942VS	2939M ⊥		2930		CH_3 ss(100)
				2930	CH_3 ss(100)
2880M	2883W ∥,⊥	2884			$C^\alpha H^\alpha$ s(99)
			2884		$C^\alpha H^\alpha$ s(99)
				2884	$C^\alpha H^\alpha$ s(99)
1655S	1658VS ∥	1657			CO s(82),CN s(10),C^αCN d(10)
			1655		CO s(82),CN s(11),C^αCN d(10)
				1645	CO s(83),CN s(12),C^αCN d(10)
				1540	NH ib(46),CN s(31),CO ib(12),C^αC s(11)
1543VW	1545VS ⊥		1538		NH ib(46),CN s(33),CO ib(11),C^αC s(10)
	1516M,sh	1519			NH ib(45),CN s(34),CO ib(11)
		1452			CH_3 ab1(47),CH_3 ab2(41), CH_3 r1(10)
			1452		CH_3 ab2(54),CH_3 ab1(31)
				1452	CH_3 ab2(59),CH_3 ab1(26)
1458S	1458VS ∥,⊥	1451			CH_3 ab2(45),CH_3 ab1(41),CH_3 r2(10)
			1451		CH_3 ab1(57),CH_3 ab2(31)
				1451	CH_3 ab1(62),CH_3 ab2(26)
1377W	1381S ⊥	1379	1379	1379	CH_3 sb(100)

1338M,sh			1349	H^{α} b1(34),NH ib(17),$C^{\alpha}C$ s(17),$C^{\alpha}C^{\beta}$ s(10)
1326S	1328M,sh ∥	1334	1345	H^{α} b1(25),H^{α} b2(20),$C^{\alpha}C$ s(17),NH ib(12)
				H^{α} b2(58),$C^{\alpha}C$ s(16)
1308M	1307S ∥,⊥	1301	1314	H^{α} b2(81)
			1308	H^{α} b2(56),H^{α} b1(23)
1278W				H^{α} b1(62)
1271W	1270M ⊥		1287	NH ib(23),NC^{α} s(18),H^{α} b1(18)
1261W	1265M,sh	1262	1278	NH ib(28),H^{α} b2(15),NC^{α} s(14),H^{α} b1(11)
				NH ib(40),H^{α} b2(28)
1167M	1170S ∥,⊥	1178		NC^{α} s(32),CH_3 r1(20),$C^{\alpha}C^{\beta}$ s(16)
			1167	$C^{\alpha}C^{\beta}$ s(32),NC^{α} s(21),CH_3 r1(15),H^{α} b1(10)
			1162	$C^{\alpha}C^{\beta}$ s(41),NC^{α} s(16),H^{α} b1(12),CH_3 r1(12)
		1115		$C^{\alpha}C^{\beta}$ s(64),CH_3 r2(15)
1105S	1108S ⊥		1103	$C^{\alpha}C^{\beta}$ s(39),CH_3 r2(18)
			1094	$C^{\alpha}C^{\beta}$ s(26),CH_3 r2(21)
1050W	1051VS ⊥		1043	CH_3 r1(47),H^{α} b1(20)
1017W	1016W ∥	1026	1037	CH_3 r1(39),H^{α} b1(22),CH_3 r2(15)
970W	968M ∥	962		CH_3 r2(28),H^{α} b1(25),CH_3 r1(24)
				CH_3 r1(34),NC^{α} s(29),CH_3 r2(17),$C^{\alpha}C$ s(15)
			955	CH_3 r2(32),NC^{α} s(20),CH_3 r1(15)
940VW			951	CH_3 r2(41),NC^{α} s(16)
908VS	909M ∥	910		CN s(23),CNC^{α} d(16),CO ib(12),CH_3 r2(11),
				CO s(10)
	893S ⊥		901	CN s(18),$C^{\alpha}C$ s(12),CO ib(12),$C^{\alpha}C^{\beta}$ s(10)
882W			896	$C^{\alpha}C^{\beta}$ s(19),$C^{\alpha}C$ s(14),CN s(14),CO ib(12),
				NC^{α} s(11)
773VW	774M		780	CO ob(42),C^{β} b1(10),CN t(10)
			767	CO ob(52),C^{β} b1(10)

(*continued*)

TABLE II (*continued*)

Observed[a]		Calculated			
Raman	ir	A	E_1	E_2	Potential Energy Distribution[b]
756W		754			CO ob(38),CN t(30)
693M	691W,sh ∥	700			$NC^{\alpha}C$ d(36),$C^{\alpha}CN$ d(26)
				675	CN t(32),CO ib(18),$C^{\alpha}C$ s(14)
662W	658S ⊥		660		CN t(37),NH ob(21),$NC^{\alpha}C$ d(12)
				637	CN t(59),NH ob(43),NH···O ib(13)
	618S ⊥		608		CN t(47),NH ob(23),CO ob(15),CO ib(12)
		589			CN t(68),NH ob(36),CO ob(26),NH···O ib(11)
530VS	526S ∥,⊥	537			CO ib(29),$C^{\alpha}CN$ d(21),$C^{\alpha}C$ s(17),C^{β} b2(17), NH ob(11)
			522		$NC^{\alpha}C$ d(31),$C^{\alpha}C$ s(14),$C^{\alpha}CN$ d(11),CO ib(11)
				492	$NC^{\alpha}C$ d(37),CO ib(17),$C^{\alpha}C$ s(16)
375S	375S ⊥		374		CO ob(16),NH ob(16),C^{β} b2(15),$C^{\alpha}CN$ d(15), CO ib(15),CNC^{α} d(10)
	~366M,sh	367			CO ob(21),C^{β} b1(17),$NC^{\alpha}C$ d(14),NH ob(13), C^{β} b2(11)
				366	C^{β} b2(49),$C^{\alpha}CN$ d(22),C^{β} b1(16)
328W	324S ⊥		326		C^{β} b2(42),C^{β} b1(19),CO ib(16)
310S				310	CNC^{α} d(30),CO ib(20),C^{β} b1(20),CO ob(17)
294M	290M ∥	307			C^{β} b2(34),CO ib(29),CNC^{α} d(15)
260M	259W,sh	264			$C^{\alpha}C^{\beta}$ t(35),C^{β} b2(14)
	240W		245		$C^{\alpha}C^{\beta}$ t(91)
				244	$C^{\alpha}C^{\beta}$ t(95)
	223VW	230			$C^{\alpha}C^{\beta}$ t(63)
209W				205	$C^{\alpha}CN$ d(27),C^{β} b2(25),C^{β} b1(12),CO ob(10)
189M	188M ⊥		197		$C^{\alpha}CN$ d(15),C^{β} b2(12),CO ob(12)
165M	163M ⊥		155		CNC^{α} d(33),$C^{\alpha}CN$ d(19),C^{β} b1(14),NH ob(14), $NC^{\alpha}C$ d(12)
159S				151	NH ob(43),CNC^{α} d(20),$NC^{\alpha}C$ d(11)
	120S ∥	136			CNC^{α} d(34),$C^{\alpha}CN$ d(21),$NC^{\alpha}C$ d(16),C^{β} b1(12)

	113M,sh ⊥		96		NH ob(24),$C^{\alpha}C$ t(20),NC^{α} t(18),CN t(18), H···O s(10)
87W	84W	94			CN t(27),NC^{α} t(23),$C^{\alpha}C$ t(22),H···O s(15), NH ob(10)
				87	NH ob(33),NH···O ib(20),C^{β} b1(12), $NC^{\alpha}C$ d(10),CNC^{α} d(10)
				49	NH ob(38),NC^{α} t(24),H···O s(23),CN t(15), C^{β} b1(13)
			40		NH ob(58),C^{β} b1(20),H···O s(11)
				38	$C^{\alpha}C$ t(53),H···O s(18)
			$\underline{(NDCH(CH_3)CO)_n}$		
		2984			CH_3 as1(98)
			2984		CH_3 as1(98)
2988	2982S			2984	CH_3 as1(94)
		2984			CH_3 as2(98)
			2984		CH_3 as2(98)
				2984	CH_3 as2(94)
2940	2941M	2930			CH_3 ss(100)
	2924M		2930		CH_3 ss(100)
				2930	CH_3 ss(100)
		2884			$C^{\alpha}H^{\alpha}$ s(99)
2886	2879W		2884		$C^{\alpha}H^{\alpha}$ s(99)
				2884	$C^{\alpha}H^{\alpha}$ s(99)
	2449VS[c]	2409	2409	2409	ND s(96)
			1648		CO s(84),CN s(13)
1652	1650VS	1647			CO s(85),CN s(13)
				1640	CO s(84),CN s(14)
				1476	CN s(35),$C^{\alpha}C$ s(22),CO ib(15)

(continued)

TABLE II (*continued*)

Observed[a]		Calculated			
Raman	ir	A	E_1	E_2	Potential Energy Distribution[b]
1477	1470M,sh	1470	1473		CN s(33),$C^{\alpha}C$ s(19),CO ib(15),CH_3 ab2(12) CN s(30),CH_3 ab2(18),$C^{\alpha}C$ s(15),CO ib(14)
1455	1454M,sh	1452	1452		CH_3 ab1(72),CH_3 ab2(17) CH_3 ab1(59),CH_3 ab2(28)
				1452	CH_3 ab1(51),CH_3 ab2(35),CH_3 r2(11)
	1439S		1445		CH_3 ab2(47),CH_3 ab1(25),CN s(10)
				1445	CH_3 ab2(43),CH_3 ab1(32)
1430		1444			CH_3 ab2(53),CN s(14),CH_3 ab1(13)
1373	1379S	1379	1379	1379	CH_3 sb(100)
				1328	H^{α} b1(54),$C^{\alpha}C^{\beta}$ s(10)
			1326		H^{α} b1(38),H^{α} b2(30)
1326	1328S	1319			H^{α} b2(74),H^{α} b1(11)
				1307	H^{α} b2(90)
1296	1293W	1299	1304		H^{α} b2(63),H^{α} b1(23) H^{α} b1(55),H^{α} b2(15)
	1178M,sh	1176			NC^{α} s(29),CH_3 r1(19),$C^{\alpha}C^{\beta}$ s(18)
	1170S		1168		$C^{\alpha}C^{\beta}$ s(26),NC^{α} s(21),CH_3 r1(16)
1158				1161	$C^{\alpha}C^{\beta}$ s(35),NC^{α} s(18),CH_3 r1(14),H^{α} b1(11)
				1147	$C^{\alpha}C^{\beta}$ s(25),CH_3 r2(20),ND ib(13)
	1140M		1136		$C^{\alpha}C^{\beta}$ s(35),CH_3 r2(21)
1095	1098M	1121			$C^{\alpha}C^{\beta}$ s(51),CH_3 r2(22)
1065	1062S	1051	1045		CH_3 r2(20),ND ib(18),H^{α} b1(17),$C^{\alpha}C^{\beta}$ s(13) CH_3 r1(29),H^{α} b1(22),CH_3 r2(15)
				1045	CH_3 r1(40),H^{α} b1(23),CH_3 r2(12)
1001	999M	984			CH_3 r1(44),ND ib(26),NC^{α} s(15),$C^{\alpha}C$ s(12)
975	974M		972		ND ib(43),CH_3 r1(23),$C^{\alpha}C$ s(10)
				961	ND ib(59),CH_3 r1(12)
				941	CH_3 r2(37),NC^{α} s(21)

945	944W		938		CH_3 r2(34),ND ib(18),NC^{α} s(15)
		929			ND ib(33),CH_3 r2(24),NC^{α} s(15)
893		892			CN s(25),CNC^{α} d(17),CO ib(11),CO s(10)
	887S		887		CN s(23),CO ib(10)
				887	CN s(21),$C^{\alpha}C^{\beta}$ s(13),$C^{\alpha}C$ s(11)
755	762M		762		CO ob(46),C^{β} b1(10)
				758	CO ob(53)
		716			CO ob(64)
682	680W,sh	685			$NC^{\alpha}C$ d(32),$C^{\alpha}CN$ d(23)
660				663	CO ib(25),$C^{\alpha}C$ s(18),$NC^{\alpha}C$ d(13)
	647M		632		CO ib(18),$NC^{\alpha}C$ d(17),CO ob(14),$C^{\alpha}C$ s(13), $C^{\alpha}CN$ d(12)
		539			CO ib(25),$C^{\alpha}C$ s(18),$C^{\alpha}CN$ d(17),NC^{α} s(12), C^{β} b2(10)
522	523S		522		$NC^{\alpha}C$ d(23),CO ib(13),$C^{\alpha}C$ s(12),NC^{α} s(10), ND ob(10)
				500	CN t(30),ND ob(26),$NC^{\alpha}C$ d(24)
				469	CN t(56),CO ib(17),ND ob(14),$NC^{\alpha}C$ d(11) $C^{\alpha}C$ s(10)
	458S		466		CN t(81),ND ob(27),ND···O ib(11)
		447			CN t(89),ND ob(55),ND···O ib(16),CO ob(11)
374		367			CO ob(21),C^{β} b1(18),$NC^{\alpha}C$ d(14),ND ob(13) C^{β} b2(11)
363			365		ND ob(22),CO ib(16),$C^{\alpha}CN$ d(15),CO ob(14), C^{β} b2(13),CN t(13),CNC^{α} d(10)
				361	C^{β} b2(49),$C^{\alpha}CN$ d(19),C^{β} b1(18)
			323		C^{β} b2(45),C^{β} b1(18),CO ib(14)
301		304			C^{β} b2(40),CO ib(28),CNC^{α} d(13)
				299	CNC^{α} d(29),CO ib(18),C^{β} b1(16),CO ob(16),

(*continued*)

TABLE II (*continued*)

Observed[a]		Calculated			
Raman	ir	A	E_1	E_2	Potential Energy Distribution[b]
					ND ob(14),CN t(12)
		260			$C^{\alpha}C^{\beta}$ t(41),C^{β} b2(10)
			244		$C^{\alpha}C^{\beta}$ t(92)
				244	$C^{\alpha}C^{\beta}$ t(95)
		229			$C^{\alpha}C^{\beta}$ t(57)
				205	C^{α}CN d(27),C^{β} b2(25),C^{β} b1(12),CO ob(10)
			195		C^{α}CN d(15),CO ob(12),C^{β} b2(11),C^{β} b1(10)
			154		CNC^{α} d(33),C^{α}CN d(19),C^{β} b1(14),ND ob(14), $NC^{\alpha}C$ d(12)
				149	ND ob(41),CNC^{α} d(19),$NC^{\alpha}C$ d(11)
		135			CNC^{α} d(34), C^{α}CN d(22),$NC^{\alpha}C$ d(16), C^{β} b1(12)
			95		ND ob(24),$C^{\alpha}C$ t(20),NC^{α} t(19),CN t(16), D···O s(10)
		94			CN t(25),NC^{α} t(24),$C^{\alpha}C$ t(22),D···O s(15)
				86	ND ob(33),ND···O ib(21),C^{β} b1(12),$NC^{\alpha}C$ d(10) CNC^{α} d(10)
				49	ND ob(37),D···O s(24),NC^{α} t(24),CN t(15) C^{β} b1(13)
			40		ND ob(57),C^{β} b1(20),D···O s(11)
				37	$C^{\alpha}C$ t(54),D···O s(18)

[a] S = strong, M = medium, W = weak, V = very, sh = shoulder, ∥ = parallel dichroism, ⊥ = perpendicular dichroism.

[b] s = stretch, as = antisymmetric stretch, ss = symmetric stretch, b = angle bend, ib = in-plane angle bend, ob = out-of-plane angle bend, ab = antisymmetric angle bend, sb = symmetric angle bend, r = rock, d = deformation, t = torsion. Only contributions 10% or greater are included.

[c] Unperturbed frequency.

adjacent chains in the crystal, which has not been included in the present force field (the β force field[2] does not require such interactions).

The amide I modes (mainly CO stretch) are very well predicted, and their downfield shift of about 8 cm^{-1} on N-deuteration is better accounted for than previously.[9] The calculated frequencies in the 1550–1370 cm^{-1} region, which contains amide II (NH in-plane bend + CN stretch) and methyl bending modes, fit the observed data satisfactorily. In fact, the present calculation shows an improvement for methyl bend modes as compared with the earlier work.[9] For example, the fit is much better for the CH_3 symmetric bend mode at ~1380 cm^{-1}, and its potential energy distribution (PED) now shows that it does not mix with any other mode.

As mentioned earlier, transition dipole coupling was included to determine the complete splitting between observed A and E_1 species amide I and amide II modes. This splitting is smaller for α-$(Ala)_n$ than for β-$(Ala)_n$.[2] This may be a general feature of helical structures: a similar trend is seen for 3_1-helical (Gly II)$_n$.[35] In amide I of α-$(Ala)_n$, the observed and predicted splittings between ir-active A and E_1 modes are zero and 2 cm^{-1} respectively, compared with 62 and 65 cm^{-1} (for B_1 and B_2 species) in β-$(Ala)_n$.[2] Although the splitting in ir-active amide II modes is larger compared with amide I, it is smaller compared to amide II splittings in β-$(Ala)_n$.[2] Our present assignment of modes in the 1550–1370-cm^{-1} region is almost the same as reported earlier,[9] but our force field gives a slightly better fit. Rabolt et al.[9] attributed the origin of bands at 1470 and 1440 cm^{-1} to a resonance between the CH_3 asymmetric bend at 1458 cm^{-1} and the unperturbed amide II′ mode (which these authors estimated at ~1451 cm^{-1}). Also, they had to reduce the force constant f(CN) by 0.500 mdyn/Å in order to fit the data in this region. There do not now seem to be compelling reasons for this interpretation. Our recent[2] ir spectrum of β-$(Ala\text{-}ND)_n$ does not indicate any splitting in the CH_3 asymmetric bend mode, and our transferring of the force field from β-$(Ala)_n$ to α-$(Ala)_n$ required no alteration in f(CN). The experimental data in this region look similar for both structures: in β-$(Ala\text{-}ND)_n$,[2] the CH_3 symmetric bend mode at ~1380 cm^{-1} remains unchanged, two new bands appear at 1488 and 1464 cm^{-1}, and the methyl asymmetric bend doublet of β-$(Ala)_n$ is replaced by one peak at ~1445 cm^{-1}. The two new peaks at 1488 and 1464 cm^{-1} are assignable to amide II′ in β-$(Ala\text{-}ND)_n$, and our calculation indicates that the two new frequencies in α-$(Ala\text{-}ND)_n$, at ~1470 and 1440 cm^{-1}, can also be assigned to amide II′, although their PED shows that there is considerably more mixing between the CH_3 asymmetric bend and CN stretch than in β-$(Ala)_n$.

The overall fit in the range 1340–940 cm^{-1} is the same as reported by Rabolt et al.,[9] but the PEDs of some bands show considerable differences. The observed bands at 1338(R), 1326(R), 1328(ir), 1308(R), and 1307(ir) are now distinctly assignable to two types of modes: the first three are due to H^α bend and $C^\alpha C$ stretch mixed with some NH in-plane bend, whereas the other two are due to pure H^α bend. In the earlier assignment,[9] these

bands were of a much more mixed type. Although the PEDs of these modes do not have large contributions from NH in-plane bend, small downward frequency shifts occur in the N-deuterated molecule, and these are reproduced moderately well. The observed bands at 1278(R), 1271(R), 1270(ir), 1265(ir), and 1261(R) are assignable to the amide III mode, both in the present and the earlier[9] work, but the present PEDs have a significantly higher contribution from NH in-plane bend. On N-deuteration, these modes shift to ~1000 cm^{-1}, which is reasonably well predicted by the present force field. The observed bands near 1170 and 1100 cm^{-1} are well predicted for α-$(Ala)_n$, and their shifts on N-deuteration, especially the new band at 1140M(ir), are reasonably well reproduced. The CH_3 rocking region of α-$(Ala)_n$, 1050 to 940 cm^{-1}, is satisfactorily reproduced. Some of the assignments in the comparable region of α-$(Ala\text{-}ND)_n$ are still uncertain.

The frequency region below 900 cm^{-1} begins to show contributions from skeletal stretches, bends, and torsions. The observed bands at 908(R), 909(ir), 893(ir), and 882(R) are mainly due to skeletal stretch and bend modes. Although they do not have any contribution from NH motion, they do show downward shifts on N-deuteration, and it is gratifying to note that the present force field predicts these shifts very well. The observed bands at 773(R), 774(ir), and 756(R) are due mainly to CO out-of-plane bend, their predicted values and shifts on N-deuteration being very satisfactorily predicted. The same is true for the pure skeletal bend mode at 690 cm^{-1}. The 670–600-cm^{-1} region is predominantly due to amide V (CN torsion + NH out-of-plane bend). The assignment in this region is almost the same as that reported earlier.[9] The major difference is the presence of an NH···O in-plane-bend contribution in the present work, this coordinate having been neglected earlier.[9] We find that the force constants associated with NH···O in-plane-bend are very crucial for amide V frequencies, and their exclusion is most likely to affect the force-field refinement. The agreement between the predicted and observed amide V′ modes is also better than previously reported.[9] The band near 530 cm^{-1} has long been considered a characteristic mode of the α-helix. The ir dichroic spectrum shows that this band has equally intense parallel and perpendicular components. Our present calculation predicts modes near this value in both the A and E_1 species, which was not the case in the earlier work.[9] Below 500 cm^{-1}, the modes are predominantly due to skeletal bends and torsions. The NH out-of-plane bend mode makes a very wide-ranging contribution in this region, where it shows significant mixing with most of the modes. Apart from slight variations in PED, our predictions in this region are almost the same as in our earlier report.[9] We note finally that, as in our earlier work,[9] we have no explanation for weak Raman bands observed at 1397, 1070, and 929 cm^{-1}.

α_{II}-Poly(L-alanine)

The relatively good agreement between observed and calculated frequencies for α_I-$(Ala)_n$ provides a basis for judging whether predicted

frequency differences for α_{II}-(Ala)$_n$ will be meaningful. The calculated normal-mode frequencies and their assignments for α_{II}-(Ala)$_n$ are presented in Table III. No experimental data on this particular form of poly(L-alanine) are available; however, since there is evidence for the presence of this conformation in proteins, it will be useful to have the predicted frequencies so that they can be used for characterizing this conformation. As noted above, a comparison of the experimental data on the amide A, I, and II modes with the theoretical predictions for the α_I and α_{II} conformations indicates that the bacteriorhodopsin in the purple membrane of *H. halobium* probably has the α_{II} conformation.[19]

The presence of weaker hydrogen bonds in α_{II} than in α_I results in higher NH stretch and amide I frequencies, and in changes in the amide II frequencies. (Since we reported our analysis of the ir spectrum of bacteriorhodopsin,[19] we have made some slight adjustments in the force field; this has shifted the calculated amide I and II frequencies by 1–2 cm^{-1}, but not modified our earlier conclusions.[19]) We note, as before,[19] that although the E_1 species amide II frequency is predicted to remain approximately the same (1538 cm^{-1} in α_I vs 1540 cm^{-1} in α_{II}), the splitting between A and E_1 is predicted to increase (19 cm^{-1} in α_I vs 25 cm^{-1} in α_{II}). The amide III frequencies decrease slightly as a result of the weaker hydrogen bond: 1262(A), 1278(E_1), and 1287(E_2) cm^{-1} in α_I vs 1260(A), 1272(E_1), and 1281(E_2) cm^{-1} in α_{II}. And while, as expected, most of the CH_3 modes are essentially unaffected by the small conformational change, CH_3 rock modes at 1026(A), 1037 (E_1), and 1043 (E_2) cm^{-1} in α_I are predicted to increase slightly, to 1031 (A), 1040 (E_1), and 1047 (E_2) cm^{-1} in α_{II}.

The effects of the small conformational difference between α_I and α_{II} show up more obviously in the lower-frequency regions. The 896 (E_2) cm^{-1} skeletal mode of α_I is predicted to shift down to 887 cm^{-1} in α_{II}. The 780 (E_1)-cm^{-1} CO out-of-plane bend mode of α_I shifts down to 770 cm^{-1} in α_{II}, while the 700 (A)-cm^{-1} skeletal bending mode of α_I is predicted to shift down to 690 cm^{-1} in α_{II}. Since the amide V modes of α_I, at 660 (E_1) and 608 (E_1) cm^{-1}, are expected to shift up in α_{II}, to 666 (E_1) and 615 (E_1) cm^{-1}, the relative separation of the 700 (A) and 660 (E_1) modes (40 cm^{-1} in α_I vs 24 cm^{-1} in α_{II}) may serve as a useful indication of the conformational change. Another sensitive feature may be the predicted inversion in order of the 374(E_1)- and 367(A)-cm^{-1} modes of α_I to 369(E_1) and 376(A) cm^{-1} in α_{II}. Finally, we note that the calculated 43-cm^{-1} separation between the 307(A)- and 264(A)-cm^{-1} modes of α_I is predicted to decrease to 28 cm^{-1} in α_{II}. Though each of the above changes may be small in itself, we would expect that their combined presence would provide strong evidence for the α_{II} conformation.

CONCLUSIONS

The present force field for α_I-(Ala)$_n$ reproduces the observed frequencies somewhat better than did our previous force field,[9] the average discrepancy for frequencies below 1700 cm^{-1} being 6.0 cm^{-1} compared with 7.6 cm^{-1}

TABLE III
Calculated Frequencies (in cm^{-1}) of α_{II}-Poly(L-alanine)

Calculated			Potential Energy Distribution[a]
A	E_1	E_2	
3288	3288	3288	NH s(99)
2984			CH_3 as1(97)
	2984		CH_3 as1(99)
		2984	CH_3 as1(98)
2984			CH_3 as2(97)
	2984		CH_3 as2(99)
		2984	CH_3 as2(99)
2930	2930	2930	CH_3 ss(100)
2884	2884	2884	$C^\alpha H^\alpha$ s(99)
1667			CO s(83),CN s(10)
	1660		CO s(83),CN s(12)
		1654	CO s(83),CN s(13)
		1543	NH ib(45),CN s(31),$C^\alpha C$ s(12),CO ib(11)
	1540		NH ib(44),CN s(32),CO ib(11),$C^\alpha C$ s(10)
1515			NH ib(43),CN s(34),CO ib(11)
		1453	CH_3 ab2(48),CH_3 ab1(37),CH_3 r2(10)
1452			CH_3 ab2(51),CH_3 ab1(36),CH_3 r1(10)
	1452		CH_3 ab2(51),CH_3 ab1(34)
1451			CH_3 ab1(52),CH_3 ab2(34),CH_3 r2(10)
	1451		CH_3 ab1(54),CH_3 ab2(34)
		1451	CH_3 ab1(51),CH_3 ab2(37)
1379	1379	1379	CH_3 sb(100)
		1347	H^α b1(40),NH ib(14),$C^\alpha C$ s(13),$C^\alpha C^\beta$ s(11)
	1346		H^α b1(26),H^α b2(23),$C^\alpha C$ s(15),NH ib(11)
1339			H^α b2(53),$C^\alpha C$ s(16)
		1315	H^α b2(78)
	1308		H^α b2(51),H^α b1(26)
1300			H^α b1(60)
		1281	NH ib(28),NC^α s(17),H^α b2(12),$C^\alpha C$ s(11),H^α b1(10)
	1272		NH ib(32),H^α b2(17),NC^α s(13)
1260			NH ib(42),H^α b2(31)
1175			NC^α s(32),CH_3 r1(21),$C^\alpha C^\beta$ s(14)
	1169		$C^\alpha C^\beta$ s(28),NC^α s(22),CH_3 r1(16),H^α b1(10)
		1164	$C^\alpha C^\beta$ s(36),NC^α s(17),CH_3 r1(13),H^α b1(12)
1114			$C^\alpha C^\beta$ s(65),CH_3 r2(15)
	1101		$C^\alpha C^\beta$ s(42),CH_3 r2(18)
		1092	$C^\alpha C^\beta$ s(29),CH_3 r2(22),NH ib(10)
		1047	CH_3 r1(48),H^α b1(19)
	1040		CH_3 r1(39),H^α b1(20),CH_3 r2(13)
1031			CH_3 r2(25),H^α b1(23),CH_3 r1(23)
961			CH_3 r1(34),NC^α s(29),$C^\alpha C$ s(16),CH_3 r2(16)
	953		CH_3 r2(35),NC^α s(21),CH_3 r1(13)
		951	CH_3 r2(44),NC^α s(16)
909			CN s(23),CNC^α d(16),CH_3 r2(15),CO ib(10)
	900		CN s(18),$C^\alpha C$ s(14),CO ib(11)
		887	$C^\alpha C^\beta$ s(19),$C^\alpha C$ s(17),CN s(15),NC^α s(12),CO ib(12)
	770		CO ob(42),CN t(14)
		759	CO ob(51)

(continued)

TABLE III (*continued*)

Calculated			Potential Energy Distribution[a]
A	E_1	E_2	
753			CO ob(39),CN t(35)
690			$NC^{\alpha}C$ d(31),$C^{\alpha}CN$ d(29),NH ob(12)
		689	CN t(34),CO ib(16),$C^{\alpha}C$ s(12)
	666		CN t(44),NH ob(26)
		651	CN t(52),NH ob(43),NH···O ib(11)
	615		CN t(33),CO ob(18),NH ob(18),CO ib(15)
592			CN t(61),NH ob(30),CO ob(28),C^{β} b1(11)
536			CO ib(33),$C^{\alpha}CN$ d(20),C^{β} b2(18),$C^{\alpha}C$ s(17),NC^{α} s(10)
	518		$NC^{\alpha}C$ d(32),$C^{\alpha}CN$ d(15), $C^{\alpha}C$ s(12)
		480	$NC^{\alpha}C$ d(38),CO ib(16),$C^{\alpha}C$ s(15)
376			C^{β} b1(22),CO ob(21),$NC^{\alpha}C$ d(18),NH ob(17)
	369		CO ob(16),C^{β} b1(15),NH ob(15),C^{β} b2(14),CNC^{α} d(12), $C^{\alpha}CN$ d(11),CO ib(11)
		363	C^{β} b2(50),C^{β} b1(21),$C^{\alpha}CN$ d(18)
	331		C^{β} b2(46),CO ib(20),C^{β} b1(14)
		308	CNC^{α} d(27),CO ib(22),CO ob(18),C^{β} b1(17)
302			C^{β} b2(50),CO ib(25)
274			$C^{\alpha}C^{\beta}$ t(20),$C^{\alpha}C$ s(10),C^{β} b2(10),CNC^{α} d(10)
		245	$C^{\alpha}C^{\beta}$ t(93)
	244		$C^{\alpha}C^{\beta}$ t(91)
233			$C^{\alpha}C^{\beta}$ t(77)
		210	$C^{\alpha}CN$ d(28),C^{β} b2(24),C^{β} b1(10)
	201		$C^{\alpha}CN$ d(14),CO ob(12),C^{β} b2(11)
	160		CNC^{α} d(36),$C^{\alpha}CN$ d(20),$NC^{\alpha}C$ d(12),C^{β} b1(11),NH ob(11)
		157	NH ob(32),CNC^{α} d(28),$NC^{\alpha}C$ d(13),$C^{\alpha}CN$ d(12)
140			CNC^{α} d(35),$C^{\alpha}CN$ d(21),$NC^{\alpha}C$ d(14),C^{β} b1(10)
106			CN t(34),H···O s(27),NC^{α} t(19),$C^{\alpha}C$ t(16)
	101		CN t(25),H···O s(22),NH ob(19),$C^{\alpha}C$ t(16),NC^{α} t(13)
		82	NH ob(24),NH···O ib(15),H···O s(13),NC^{α} t(12),$C^{\alpha}C$ t(10)
		51	NH ob(67),C^{β} b1(24),H···O s(20),CN t(18),NC^{α} t(11)
	40		NH ob(67),C^{β} b1(24),H···O s(19),$NC^{\alpha}C$ d(10),NC^{α} t(10)
		35	$C^{\alpha}C$ t(51),NH···O ib(15),H···O s(14),NC^{α} t(12)

[a] s = stretch, as = antisymmetric stretch, ss = symmetric stretch, b = angle bend, ib = in-plane angle bend, ob = out-of-plane angle bend, ab = antisymmetric angle bend, sb = symmetric angle bend, r = rock, d = deformation, t = torsion. Only contributions 10% or greater are included.

[for α_I-(Ala-ND)$_n$ the average discrepancy is 5.9 cm^{-1}]. This level of agreement compares with those for our recent refinements of (Gly I)$_n$ (5.4 cm^{-1})[1] and β-(Ala)$_n$ (4.6 cm^{-1}).[2] It therefore provides a good basis for examining the effects of small conformational changes on the vibrational spectrum.

This force field was transferred unchanged to the calculation of the normal modes of the α_{II}-helix, except for small alterations in f(CO), f(NH), and f(H···O) (small changes in other hydrogen-bond force constants are probably warranted, but these cannot be determined at this time because of lack of data). This transfer is probably justified, since there is such a

small conformational difference between the α_I- and α_{II}-helices. Nevertheless, there are significant predicted differences between the vibrational frequencies of these two structures, not only in the amide I and II regions as a result of different transition dipole coupling contributions, but particularly in the conformation-sensitive region between 900 and 200 cm^{-1} (where changes in hydrogen-bond force constants have no influence on the frequencies). This result emphasizes the sensitivity of the vibrational spectrum to even small changes in conformation of the polypeptide chain.

The predicted spectral differences between the α_{II}- and α_I-helices indicate that the helices in the bacteriorhodopsin of *H. halobium* are probably α_{II}-helices,[19] which, in turn, led to the suggestion[19] that the helix itself may be the proton "conductor" in this protein.

We are indebted to Dr. Bernard Lotz for discussions that led to the detailed studies reported here. We appreciate the contributions of Dr. Jagdeesh Bandekar to the early stages of this work. This research was supported by National Science Foundation Grants PCM-7921652 and DMR-7800753.

References

1. Dwivedi, A. M. & Krimm, S. (1982) *Macromolecules* **15,** 177–185.
2. Dwivedi, A. M. & Krimm, S. (1982) *Macromolecules* **15,** 186–193; (1983) **16,** 340.
3. Bandekar, J. & Krimm, S. (1979) *Proc. Natl. Acad. Sci. USA* **76,** 774–777.
4. Bandekar, J. & Krimm, S. (1979) in *Peptides: Structure and Biological Function. Proceedings of the Sixth American Peptide Symposium*, Gross, E. & Meienhofer, J., Eds., Pierce Chemical Co., Rockford, Ill., pp. 241–244.
5. Krimm, S. & Bandekar, J. (1980) *Biopolymers* **19,** 1–29.
6. Bandekar, J. & Krimm, S. (1980) *Biopolymers* **19,** 31–36.
7. Maxfield, F. R., Bandekar, J., Krimm, S., Evans, D. J., Leach, S. J., Némethy, G. & Scheraga, H. A. (1981) *Macromolecules* **14,** 997–1003.
8. Bandekar, J., Evans, D. J., Krimm, S., Leach, S. J., Lee, S., McQuie, J. R., Minasian, E., Némethy, G., Pottle, M. S., Scheraga, H. A., Stimson, E. R. & Woody, R. W. (1982) *Int. J. Pept. Protein Res.* **19,** 187–205.
9. Rabolt, J. F., Moore, W. H. & Krimm, S. (1977) *Macromolecules* **10,** 1065–1074.
10. Miyazawa, T. (1961) *J. Polym. Sci.* **55,** 215–231.
11. Némethy, G., Phillips, D. C., Leach, S. J. & Scheraga, H. A. (1967) *Nature* **214,** 363–365.
12. Blake, C. C. F., Mair, G. A., North, A. C. T., Phillips, D. C. & Sarma, V. R. (1967) *Proc. R. Soc. London, Ser. B* **167,** 365–377.
13. Birktoft, J. J. & Blow, D. M. (1972) *J. Mol. Biol.* **68,** 187–240.
14. Carter, Jr., C. W., Kraut, J., Freer, S. T., Xuong, N., Alden, R. A. & Bartsch, R. G. (1974) *J. Biol. Chem.* **249,** 4212–4225.
15. Parrish, Jr., J. R. & Blout, E. R. (1972) *Biopolymers* **11,** 1001–1020.
16. Arnott, S. & Dover, S. D. (1967) *J. Mol. Biol.* **30,** 209–212.
17. Rothschild, K. J. & Clark, N. A. (1979) *Biophys. J.* **25,** 473–487.
18. Rothschild, K. J. & Clark, N. A. (1979) *Science* **204,** 311–312.
19. Krimm, S. & Dwivedi, A. M. (1982) *Science* **216,** 407–408.
20. Colonna-Cesari, F., Premilat, S. & Lotz, B. (1975) *J. Mol. Biol.* **95,** 71–82.
21. Ramachandran, G. N. & Sasisekharan, V. (1968) *Adv. Protein Chem.* **23,** 283–438.
22. Moore, W. H. & Krimm, S. (1976) *Biopolymers* **15,** 2465–2483.

23. Fanconi, B., Tomlinson, B., Nafie, L., Small, E. W. & Peticolas, W. (1969) *J. Chem. Phys.* **51,** 3993–4005.
24. Krimm, S. & Abe, Y. (1972) *Proc. Natl. Acad. Sci. USA* **69,** 2788–2792.
25. Moore, W. H. & Krimm, S. (1975) *Proc. Natl. Acad. Sci. USA* **72,** 4933–4935.
26. Bamford, C. H., Elliott, A. & Hanby, W. E. (1956) *Synthetic Polypeptides*, Academic Press, New York, p. 143.
27. Elliott, A. (1954) *Proc. R. Soc. London, Ser. A* **226,** 408–421.
28. Frushour, B. G. & Koenig, J. L. (1974) *Biopolymers* **13,** 455–474.
29. Koenig, J. L. & Sutton, P. L. (1969) *Biopolymers* **8,** 167–171.
30. Itoh, K. & Shimanouchi, T. (1970) *Biopolymers* **9,** 383–399.
31. Itoh, K., Nakahara, T., Shimanouchi, T., Oya, M., Uno, K. & Iwakura, Y. (1968) *Biopolymers* **6,** 1759–1766.
32. Itoh, K., Shimanouchi, T. & Oya, M. (1969) *Biopolymers* **7,** 649–658.
33. Fanconi, B. (1973) *Biopolymers* **12,** 2759–2776.
34. Fanconi, B., Small, E. W. & Peticolas, W. L. (1971) *Biopolymers* **10,** 1277–1298.
35. Dwivedi, A. M. & Krimm, S. (1982) *Biopolymers* **21,** 2377–2397.
36. Krimm, S. & Dwivedi, A. M. (1982) *J. Raman Spectrosc.* **12,** 133–137.

Received January 20, 1983
Accepted October 17, 1983